NEW DEVELOPMENTS IN COMPRESSOR AERODYNAMICS

by

Dr. Meherwan P. Boyce
Director, Gas Turbine Laboratories
Texas A&M University

Dr. Boyce is the director of Gas Turbine Laboratories, and Environmental Tunnel Facilities, and an assistant professor in mechanical engineering. He has several years of research and industrial experience. His last industrial position was as chief aerodynamist with Fairchild Hiller Corp.

He received a B.S. (Mechanical Engineering) degree from South Dakota School of Mines and Technology in 1962, a M.S. (Mechanical Engineering) degree from State University of New York in 1964, a diploma in business administration from International Correspondence School in 1966, and a Ph.D. (Mechanical Engineering) degree from University of Oklahoma in 1969. He is a member of several professional and honorary societies and a registered professional engineer in the state of Texas. Dr. Boyce has authored several significant papers and technical reports in the area of fluid mechanics and turbomachinery.

ABSTRACT

This paper deals with the new developments in compressor aerodynamics. The emphasis in this paper is on the various aerodynamic developments that have led to better compressor performance. An outline of a new technique to obtain the blade loading in a radial flow compressor has been discussed here.

The losses presented in this paper are for the radial flow compressor and are divided into two groups: (1) losses encountered in the rotor, and (2) losses encountered in the stator. Results of flow visualization studies are given so that better understanding of the flow phenomena can be attained. This is essential, if the goals of high pressure, high efficiencies, and large surge-to-stall margins are to be obtained. The feasibility study of a radial inward flow compressor is also discussed. An extensive bibliography is presented for the readers.

INTRODUCTION

The development of compressor technology in the past 20 years has advanced rapidly from an art to a science. The goal of this paper is to show some of the most recent developments in compressor aerodynamics, and to indicate the future trends in this area. The paper will deal mainly with the developments in the area of centrifugal compressors since this is the most widely used type of compressor in the process industry. However, trends in the area of axial flow compressor aerodynamics, will also be discussed briefly.

[1]Numbers in parentheses refer to REFERENCES at end of paper.

Studies at the Texas A&M University Gas Turbine Laboratories have been directed towards better understanding the complex flow phenomena encountered in a compressor. This has been done by developing new analytical methods to evaluate blade loading and losses encountered in a compressor. The analytical methods are further supported by using flow visualization techniques to better understand and explain the complicated flow phenomena in a compressor.

Recent trends in both axial and radial compressors is to develop high pressure ratio compressors without a loss in efficiency and a reduction in surge-to-stall margins. The trend to this high pressure results in the flow in the compressor to be supersonic. Thus, the area of supersonic aerodynamics is one of the future trends that should be investigated.

The emphasis in this paper will be to present the various aerodynamic developments that have led to better the efficiency of various type of compressors. An extensive bibliography is presented for the readers who would like to investigate any area in greater detail.

BLADE LOADING ANALYSIS

Many papers, over the last two decades, have dealt with the problem of blade loading in radial flow compressors (1-5).[1] The papers have all considered the flow in the rotor to be inviscid and the process to be isentropic. The inclusion of viscous terms in the momentum equation for a rotating coordinate system leads to an equation which does not lend itself easily to a solution. Thus, the method of superimposing a boundary layer on the solution of an inviscid flow calculation has been found to be very attractive. However, neglecting of entropy terms in the momentum equation is unnecessary.

The blade loading analysis in this paper deals with the solution of the momentum equation in a rotating coordinate system. All the terms are retained and a more accurate solution is obtained. The advantage of this method becomes very obvious when the inlet flow conditions are not homentropic, such as is usually the case for the inlet of the second stage. The differential equation obtained is solved in a rigorous manner.

The method outlined here is a quasi-three-dimensional solution. It is composed of two solutions, one in the meridional plane (hub-to-shroud solution) and the other in the θ plane (blade-to-blade solution). This approach has been traditional and gives an accurate three-dimensional picture of the flow in such a passage.

The solution of entire blade loading is obtained in three steps. First the passage is divided into a number of streamtubes and their coordinates are obtained. The assumptions are being that all streamtubes carry the same

mass flow rate. The second step is the calculation of the velocity gradient in the hub-to-shroud plane, the third step being the blade-to-blade solution.

Once the meridional plane is divided into preliminary streamlines, the calculation in the hub-to-shroud plane can be initiated. The combination of the momentum and energy equations in the meridional plane results in a differential equation of the form as shown below from reference (6)

$$\frac{1}{2}\frac{dW^2}{dn} = aW^2 - bW + c \qquad (1)$$

where

$$a = \frac{\cos^2\beta}{r_c} - \frac{\sin^2\beta\cos\alpha}{r} - \frac{B\cos\beta\sin\beta\sin\alpha}{r}$$

$$b = 2\omega\sin\beta\cos\alpha + B\cos\beta\left(\frac{dW_\theta}{dm} + 2\omega\sin\alpha\right)$$

$$c = \frac{1}{p_i}\frac{dP_i}{dn} + \frac{d}{dn}\left(\frac{W_i^2}{2}\right) - r_i\,\omega^2\cos\alpha_i$$

$$\text{and } B = r\frac{\partial O}{\partial Z}\sin\alpha - r\frac{\partial O}{\partial r}\cos\alpha$$

The solution for equation (1) may be written as follows:

if $(b^2 - 4ac) > 0$, then

$$\left(\frac{W_{j-1} - J}{W_j - J}\right)\left(\frac{W_j - L}{W_{j-1} - L}\right)^{L/J} = e^{a\Delta n(-J+L)/J} \qquad (2)$$

where

$$J = \frac{b - \sqrt{b^2 - 4ac}}{2a}$$

$$L = \frac{b + \sqrt{b^2 - 4ac}}{2a}$$

or if $(b^2 - 4ac) < 0$, then

$$\ln\left(\frac{aW_j^2 + (-b)W_j + c}{aW_{j-1}^2 + (-b)W_{j-1} + c}\right) - \frac{-2b}{\sqrt{4ac - b^2}}\left[\tan^{-1}\left(\frac{2aW_j + (-b)}{\sqrt{4ac - b^2}}\right) - \tan^{-1}\left(\frac{2aW_{j-1} + (-b)}{\sqrt{4ac - b^2}}\right)\right] = 2a\Delta n \qquad (3)$$

Thus, knowing the characteristics of the previous streamline, the value of the adjacent streamlines may be obtained. The value of the relative velocity obtained in equations (2) and (3) are exact solutions of equation (1).

With the meridional plane analysis completed, the next step is the blade-to-blade solution. The velocities and pressures on the trailing and driving faces are obtained by combining the energy and momentum equation in the blade-to-blade plane as shown:

$$(W_D + W_T) = 2W \qquad (4)$$

$$(W_T - W_D) = \cos\beta\left(\frac{2\pi r - Zt_\theta}{Z}\right)\left(\frac{dW_\theta}{dm} + \frac{W}{r}\sin\beta\sin\alpha + 2\omega\sin\alpha\right) \qquad (5)$$

$$\frac{p}{p_{oi}} = \left(\frac{T}{T_o}\right)^{\gamma/\gamma-1}\left(1 + \frac{UV - U_iV_i}{c_p T_{oi}}\right)^{K/K-1} \qquad (6)$$

LOSSES

The accurate calculation and proper evaluation of the losses is as important as the calculation of the blade loading parameter since unless the proper parameters are controlled efficiency drops.

The evaluation of various losses is a combination of experimental results and theory. The losses presented here are for the radial flow compressor; however, they are general enough that with slight modifications they may be used for axial flow compressors. The losses are divided into two groups: (1) losses encountered in the rotor, and (2) losses encountered in the stator.

The losses are usually expressed as a loss of heat or enthalpy. A convenient way to express them is in a nondimensional manner with reference to the inlet velocity. The theoretical total head available (q_{tot}) is equal to the head available from the energy equation plus the head which is lost due to disk friction and due to any recirculation of the air back into the rotor from the diffuser

$$q_{tot} = q_{th} + \Delta q_{DF} + \Delta q_{rc} \qquad (7)$$

The adiabatic head that is actually available at the rotor discharge is equal to the theoretical head minus the heat losses due to the shock in the rotor, the blade loadings, the clearance between the rotor and the shroud, and the viscous losses encountered in the flow passage

$$q_{ia} = q_{th} - \Delta q_{sh} - \Delta q_{BL} - \Delta q_c - \Delta q_{SF} \qquad (8)$$

Therefore, the polytropic efficiency in the impeller is

$$\eta_{imp} = \frac{q_{ia}}{q_{tot}} \qquad (9)$$

The calculation of the over-all stage efficiency now has to include the losses encountered in the diffuser. Thus, the over-all actual adiabatic head attained would be the actual adiabatic head of the impeller minus the head losses encountered in the diffuser due to wake caused by the impeller blade, the loss of part of the kinetic head at the exit of the diffuser, and the loss of head due to the frictional forces encountered in the vaned or vaneless diffuser space

$$q_{oa} = q_{ia} - \Delta q_w - \Delta q_{ex} - \Delta q_{OSF} \qquad (10)$$

The calculation of the theoretical head is based on the Eulerian turbine equation

$$E = (U_1V_{\theta 1} - U_2V_{\theta 2}) \quad . \qquad (11)$$

Since the losses are presented in a nondimensional manner, the theoretical head is thus equal to

$$q_{th} = \frac{U_1V_{\theta 1}}{U_1^2} - \frac{U_2V_{\theta 2}}{U_1^2} \quad . \qquad (12)$$

The individual losses can now be computed. These losses are broken up into two major categories; (1) losses in the rotor, and (2) losses in the diffuser.

ROTOR LOSSES

The rotor losses as mentioned previously are divided further into various categories. The following is the analysis of each of these losses.

Shock in Rotor Loss

This loss is due to the shock occurring at the rotor inlet. The inlet of the rotor blades should be wedge-like so as to obtain a weak oblique shock and then should gradually be expanded to the blade thickness so as to avoid another shock. The loss is computed and based on the work by Vavra (7) for axial flow cascades.

$$\Delta q_{sh} = 1 - \left(\frac{W_{sh}}{W_1}\right)^2 - \frac{2}{\gamma - 1}\frac{1}{M^2_{rel}}\left[\left(\frac{p_2}{p_1}\right)^{\frac{\gamma-1}{\gamma}} - 1\right] \tag{13}$$

If the blades were blunt, this would lead to a bow shock which would cause the flow to detach from the blade wall.

Disk Friction Loss

This is the loss due to the frictional torque on the back surface of the rotor. This loss is the same for a given size disk whether it is used for a radial inflow compressor, a radial outflow compressor, or a radial inflow turbine. In many cases, the losses in the seals, bearings, and gear box are also lumped in with this loss, and the entire loss can be called an external loss. However, in this study, the disk friction loss, excluding mechanical seal and bearing losses, is calculated. This loss is based on the work done by Watabe (8, 9, 10).

$$\Delta q_{DF} = \frac{c_f \left(1 + \frac{\rho_1}{\rho_2}\right)}{2\left(\frac{W_z}{U_2}\right) q_{th}\left(\frac{d_{s2}}{d_{s1}}\right)^2\left[1 - \left(\frac{d_{h1}}{d_{s1}}\right)^2\right]} \tag{14}$$

where

$c_f = 0.0622\ Re^{-0.2}$ (turbulent $Re > 3 \times 10^5$)

$c_f = 2.67\ Re^{-0.5}$ (laminar $Re < 2 \times 10^5$)

From the foregoing equations, it is obvious that the gap between the housing and the rotor has not been considered. Work by C. Schmieden (11) and later by F. Schultz-Grunow (12) showed that unless the gap was of the order of magnitude of the boundary layer, the effect of the gap size was negligible. A point of interest that should be indicated here is that the disk friction in a housing is less than that on a free disk. This is due to the existence of a "core" which rotates at half the angular velocity.

Diffusion Blading Loss

This loss arises because of negative velocity gradients in the boundary layer. This deceleration of the flow increases the boundary layer and gives rise to separation of the flow. In the case of the radial inflow compressor, this loss is compounded by the fact that the centripetal force acts against the flow direction. Thus, this inverse pressure gradient, combined with the inverse pressure gradient a compressor normally works against, gives rise to a rather significant loss. This loss is based on the work done by Balje (13, 14). Here he modifies the general Truckenbrodt equation and applies it to the case of a centrifugal impeller to calculate the momentum thickness

$$\delta = \frac{\left(\frac{A}{4 + \frac{2}{n}}\right)^{\left(\frac{n}{n+1}\right)}}{Re^{\left(\frac{1}{n+1}\right)}} 2\left[\frac{1 - \left(\frac{1}{\mu}\right)^{\left(4 + \frac{2}{n}\right)}}{1 - \left(\frac{1}{\mu}\right)}\right]^{\frac{n}{n+1}} \tag{15}$$

where A and n are constants and depend on the Reynolds number. (n = 1 and A = 0.46 for laminar flow; n = 6 and A = 0.076 for turbulent flow).

The diffusion loss can now be computed by using the equation developed for the axial flow compressor

$$q_{DF} = 2\delta \frac{\sigma}{\sin\beta_2}\left(1 + \frac{1}{2}\delta\frac{\sigma H^2}{\sin\beta_2}\right) \tag{16}$$

where H = form factor (1.18 to 1.3) and σ (solidity factor) is given by the following equation:

$$\sigma = \frac{r_1 - r_{s2}}{\frac{2\pi}{Z}(r_1 + r_{s2})} + \frac{b_i}{\frac{\pi}{Z}(r_{s2} + r_1)} \tag{17}$$

a more accurate value of solidity could be obtained by conformaly mapping the centrifugal impeller to an axial flow impeller, since equation (19) is based on axial flow data. This has been done by Boyce and Bale (15).

Clearance Loss

The clearance loss is defined as the loss due to the leak from the driving to the trailing face as shown in Figure 1. This loss may be quite substantial. The leaking flow undergoes a large expansion and contraction due to temperature variation across the clearance gap affecting both the leaking flow and the stream into which it discharges. Work on this loss has been done by many individuals such as Eckert (16), by Sherstyuk et. al (17), and the work by Vasil'ev et al (18) which seems to give the best correlation to experimental data. The following is the empirical equation presented by them

$$\Delta q_{CL} = 0.17\ q_{th}\ \bar{\delta} \tag{18}$$

where $\bar{\delta} = S/b_i$.

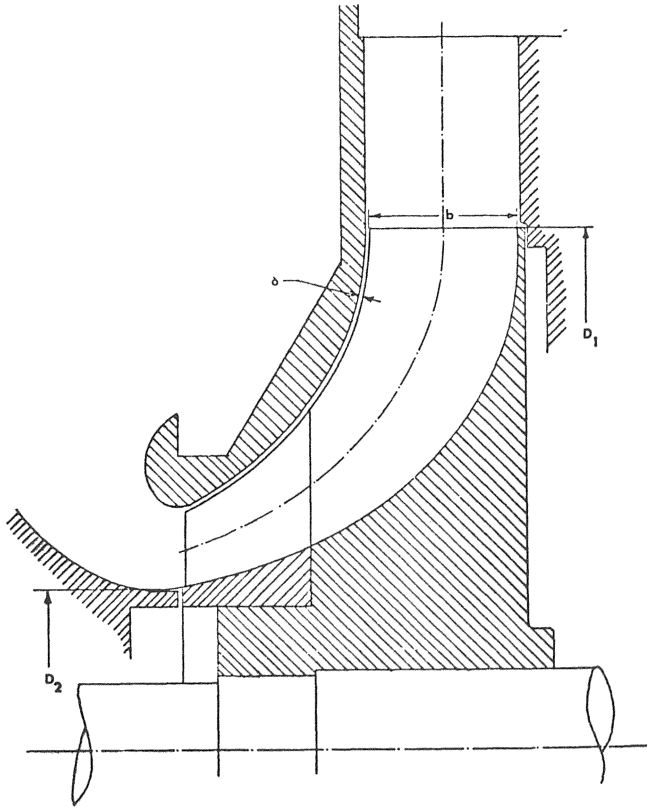

Figure 1. Section of Impeller Showing the Clearance.

Skin Friction Loss

Skin friction loss is defined as loss due to the shear forces on the impeller wall which are mostly due to turbulent friction. This type of loss is usually determined by considering the flow area as an equivalent circular cross section with a hydraulic diameter, d_H. The hydraulic diameter is given by the following equation

$$d_H = \frac{4 \times \text{cross sectional area}}{\text{wetted perimeter}}$$

which, for the case of radial outflow compressor, is

$$d_H = \frac{2\left(\frac{\pi}{4}(d_{s2}^2 - d_{h2}^2)\cos\beta_2\right)}{\pi(d_{s2} + d_{h2})\cos\beta_2 + 2Z(d_{s2} - d_{h2})} + \frac{\pi d_1 b_i \cos\beta_1}{\pi d_1 \cos\beta_1 + Z b_i} \qquad (19)$$

It is now possible to calculate this loss based on the well-known "pipe flow pressure loss equation" and the work done by Schiller (25) and Nikuradse (26).

$$\Delta q_{SF} = 4\, K_{SF}\, C_f \left(\frac{l}{d_H}\right) \frac{1}{2} \left(\frac{Wavg}{U_1}\right)^2 \qquad (20)$$

where

K_{SF} = 1.4 an empirical constant

$C_f = 0.0622\ Re^{-0.2}$ $(Re > 3 \times 10^5)$

$C_f = 2.67\ Re^{-0.5}$ $(Re \quad 2 \times 10^5)$

$Re_a = \frac{Wavg \times d_H}{\nu}$

l = meridional path length

$Wavg$ = mean square relative velocity

ν = kinematic viscosity

STATOR LOSSES

Impeller Recirculating Loss

This loss occurs due to the back flow into the impeller exit of a compressor, and is a direct function of the air exit angle (α_2). This loss has been based on considerable test data.

$$\Delta q_{cr} = 0.02\ D^2\ (\tan\alpha_2)^{0.5}$$

where

D = Diffusion factor

Wake Mixing Loss

This loss is due to the impeller blades, causing a wake in the vaneless space behind the rotor. This loss is minimized in a diffuser which is symmetric around the axis of rotation, since, once again, there are no experimental results to go by and this loss in the case of a radial outflow compressor is of the order of one half of one percent. This loss would be less for the case of a diffuser with axial symmetry.

Vaneless Diffuser Loss

Vaneless diffuser loss may be developed by considering the coefficient of friction to be constant and the absolute flow angle to be constant.

$$\Delta q_{VLD} = \frac{4c_f}{12} \times \frac{d_{2avg}}{b_i} \times \frac{1}{\cos\alpha_{avg}} \left[1 - \left(\frac{d_2}{d_3}\right)^{1.5}\right] \qquad (21)$$

where

$$C_f = 0.0592\ Re^{-0.2} \left(1 + \frac{\gamma - 1}{2} M^2\right)^{-0.45}$$

$$\frac{V_3}{V_2} = \left(\frac{d_2}{d_3}\right)^{1.25}$$

$$Re = \frac{V_{avg} \times \text{length of passage}}{\nu}$$

M = Mach no.

Vaned Diffuser Loss

Vaned diffuser loss is based on the conical diffuser test results

$$\Delta q_{vd} = \frac{K_{vd}}{2} \left[0.07 + 0.0076 \left(\frac{V_3}{V_4} - 1\right)^3\right] \left[\frac{V_3}{U_1}\right] \qquad (22)$$

where K_{vd} accounts for the nonuniformity of flow entering the diffuser. It is a function of impeller blade load-

ing and the vaneless space radius ratio as found experimentally.

$$K_{vd} = 1 + 0.44 \left(1 - \frac{V_3}{V_4}\right)^3 \left[1 - \left(\frac{d_4}{d_3} - 1\right)^{1/3}\right]$$

Exit Loss

The exit loss assumes that one-half of the kinetic energy leaving the vaned diffuser is lost.

$$\Delta q_{ex} = \tfrac{1}{4}\left(\frac{V_4}{U_1}\right)^2 \qquad (23)$$

FLOW VISUALIZATION STUDIES

The flow in a compressor is complex. Better understanding of this flow phenomena is essential, if the goals of high pressure, high efficiencies and large surge-to-stall margins are to be obtained.

The flow must be visualized three-dimensionally. Unless the three-dimensional flow is understood and a new mathematical model obtained, no further progress can be made in the theoretical computational area. The present theoretical methods fail in analyzing the flow near the impeller tips. This is a very critical point in the impeller since a majority of the flow reversal problems are initiated at the tips. Flow visualization studies conducted by Boyce (19) and Fowler (20, 21) are the most recent papers in this area. These experimenters have attempted to visualize in a three dimensional manner the flow in a centrifugal impeller. The results of these studies indicate that the theoretical methods forwarded by Boyce and Bale (6), Senoo and Nakase (22, 23), Stockman and Kramer (5), Katsanis (24), do not accurately predict the flow in the "blade to blade" plane. There are many explanations of this phenomena; the most accepted one is that current methods presently do not account for the three dimensional boundary layer.

The apparatus used by Boyce (19) included a centrifugal impeller made of a highgrade steel and chrome

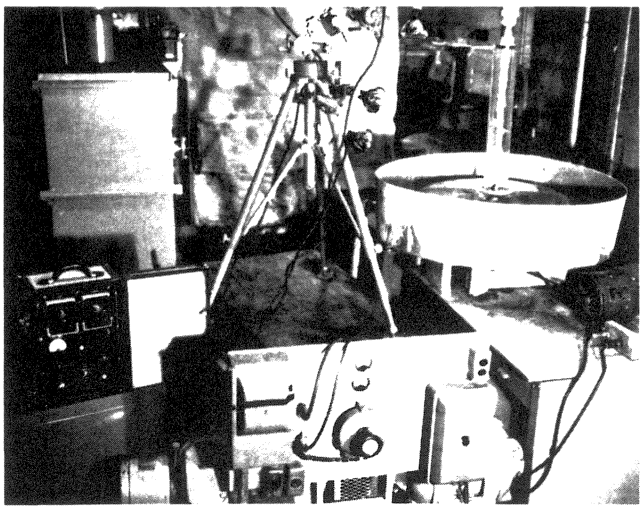

Figure 2. Experimental Setup.

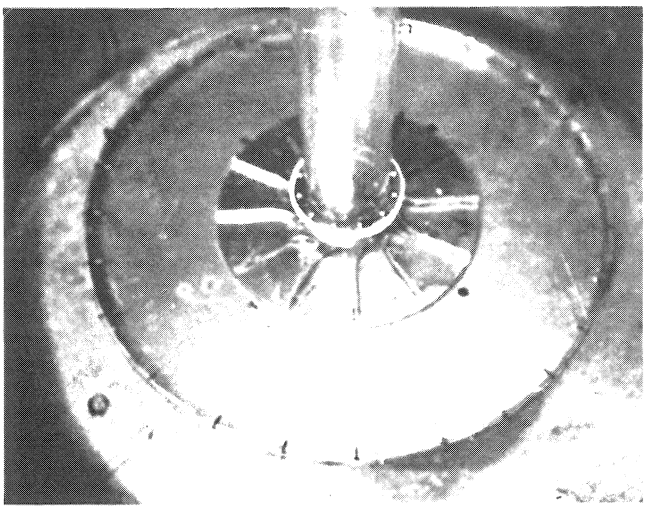

Figure 3. Impeller and Shroud.

plated to a very highly reflective finish, covered with a shroud made of plexiglass. The impeller mounted with a vertical axis on a specially constructed base. The shaft was connected at one end to the impeller and at the other end to a pulley, which was in turn connected by a V-belt to a variable-speed d-c motor (Figures 2 and 3).

The entire apparatus was surrounded by a trough designed to catch the outflowing water. The water discharge was regulated at the end of the diffuser by a band of brass which had holes along its length. These matched the holes in the plexiglass band (which encircled the shroud) in number and size. To regulate the flow, the brass band was slipped around until it partially covered the holes on the plexiglass band. An inlet pipe of plexiglass was attached to the shroud. It was connected to a large overhead tank which was about 7 ft. above the model. The tank was designed to give a constant head of water. One foot from where the plexiglass inlet pipe was attached to the shroud, a hypodermic needle and syringe were joined to the outside of the tubing and, through it a neutral specific gravity of dibutyl phthalate and kerosene colored black for better contrast with the impeller was injected.

The high speeds at which the motion pictures were taken enabled the blades to be visualized without blurring when projected at lower speed. An adjacent pair of blades was marked with black stripes to indicate a blade passage (Figure 4). All calculations were carried out in this passage.

The distance of the globule from the rim of the impeller in the horizontal plane and the distance of the globule from the back of the impeller in the vertical plane were measured directly from the enlargement. The size of the blade on the enlargement and the actual size of the blade were always correlated so as to calculate the actual distance. This keeps the position of the globule, with respect to the actual height of the blade, in correct perspective.

The projected height of the globule above the impeller surface will always be half the distance between

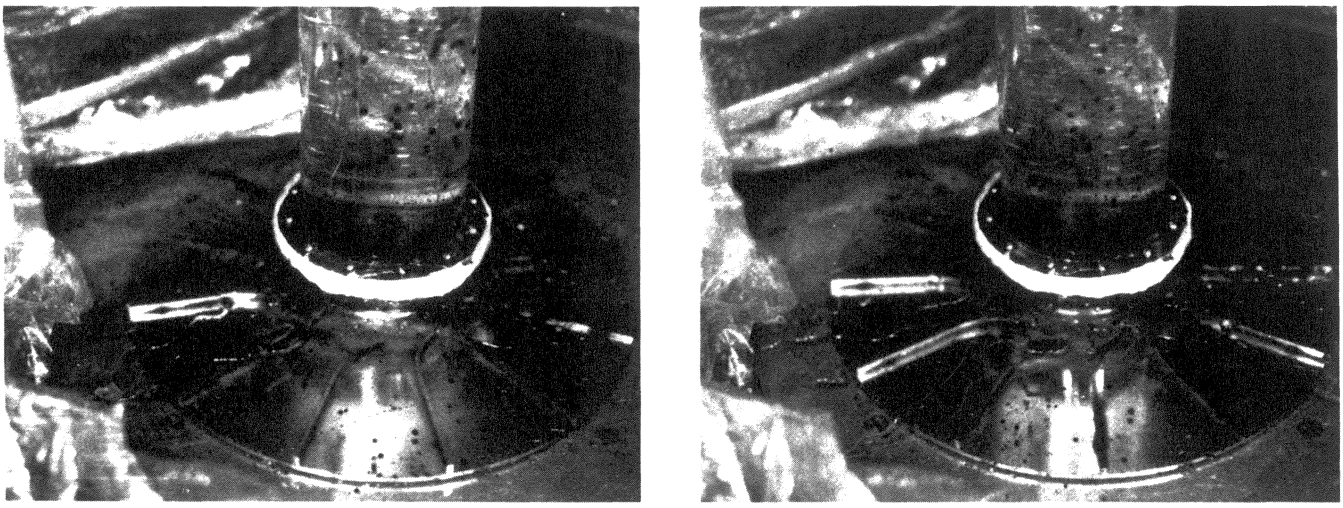

Figure 4. Impellers Showing Beads Used to Map Out Flow.

the globule and its reflection-a/2. Therefore, the actual distance of the globule above the impeller surface is half the measured distance between the globule and the reflection times the ratio between the actual height of the blade and the measured height. The angle of projection introduced by the camera's location is automatically compensated by this technique. The change in distance between the globule and its reflection was used to calculate the meridional velocity in the axial plane when the speeds of the impeller and the motion picture are known.

The visualization technique discussed herein diagnoses the flow in both the impeller and the meridional planes. The tests conducted with water as the fluid medium, so as to facilitate the flow visualization technique. An impeller designed for air can be tested using water as the medium if the dimensionless parameters, Reynolds number, and specific speed are held constant:

$$\text{Reynolds number} = \frac{\rho_{air} V_{air} D}{\mu_{air}} = \frac{\rho_{water} V_{water} D}{\mu_{water}} \tag{24}$$

$$\text{Specific speed} = \frac{Q_{air}}{N_{air} D^3} = \frac{Q_{water}}{N_{water} D^3} \tag{25}$$

where ρ = density of medium, V = velocity, D = diameter of impeller, μ = viscosity, and N = speed. Using this assumption, we can apply this method of flow visualization to any working medium.

The flow, as observed in the impeller plane near the shroud, seemed to flow in a recirculating spiral (Figure 5). The streamlines observed in this figure do not cross but are actually in different planes. This observed phenomenon, the recirculating spiral, is not due to any analytical definition of the fluid flow but to the shearing effect the stationary shroud has on an impeller. It is probable that this phenomenon would not be observed in a rotating shroud impeller.

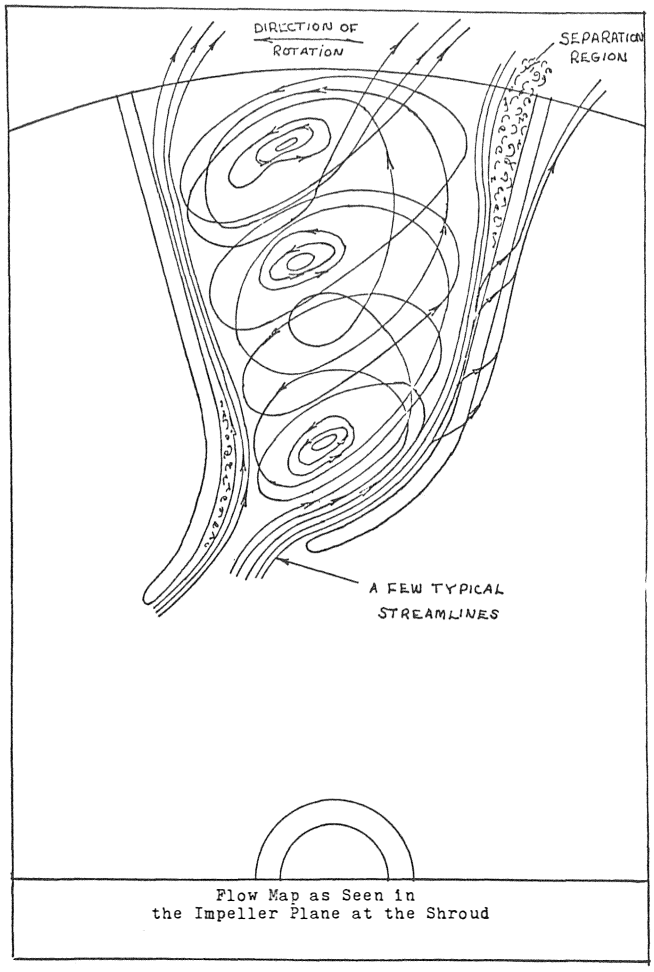

Figure 5. Flow Map as Seen in the Impeller Plane at the Shroud.

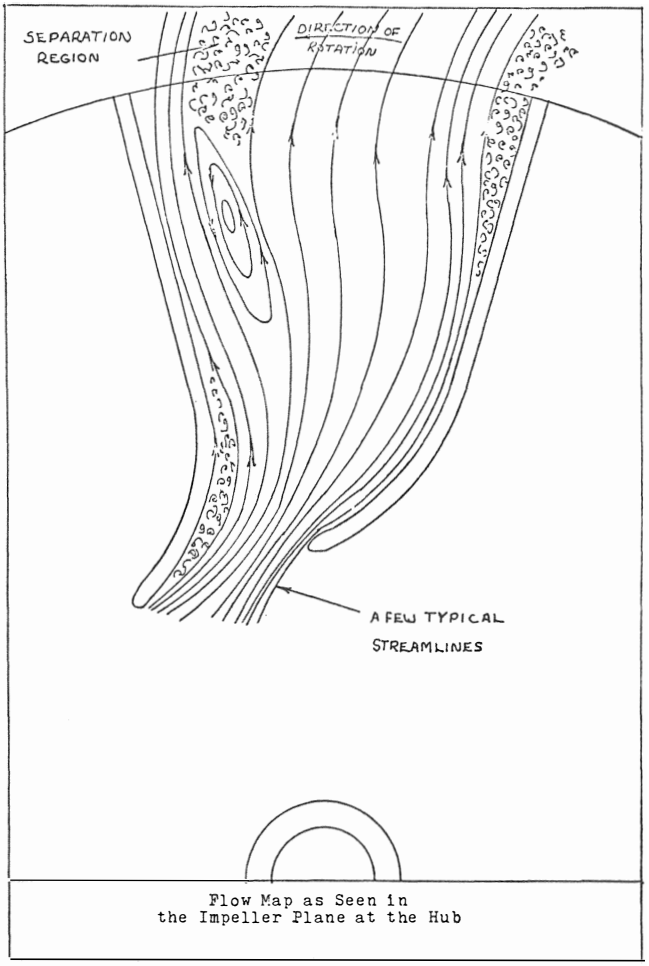

Figure 6. Flow Map as Seen in the Impeller Plane at the Hub.

The flow in the impeller plane near the hub followed the geometry of the impeller more closely (Figure 6). There was some leakage observed over the tip of the blades due to the clearance between the impeller and the shroud. Separations regions were noted at the inducer section on the suction side of the blade and near the tip on the pressure side of the blade. The separation regions near the inducer section may be attributed to the flow dividing itself at the leading edge of the blade. Very little can be done to avoid this loss. The separation near the tip is caused by the build-up of boundary layer, which in turn is caused by the slow-moving fluid adjacent to the blade. Boundary layer slots, as suggested in this paper, are one way in which these separation regions may be reduced. They enable the slow moving fluid to be bled off and its place to be taken by a faster moving stream of fluid.

Visualization of flow in the meridional plane is also diagnosed. To calculate the direction and magnitude of the velocity in this plane, the reflecting technique is necessary. The flow in this plane has a gentle wave (Figure 7). Secondary flow regions were encountered near the inducer and tip of the impeller.

A significant flow visualization technique has yet to be developed to visualize three dimensionally the flow in an axial flow compressor. Recent work in holography may open up an entire new area in this field.

BOUNDARY LAYER CONTROL

Boundary-layer control is not a new approach and is being used in industry more than ever before. It has been used with success on airfoil designs when it has delayed separation, thus giving a larger usable angle of attack. Control of the flow over an airfoil has been accomplished typically in two ways; first, by using slots through the airfoil; and second, by injecting a stream of fast-moving air.

Separation regions are also encountered in the centrifugal impeller as shown in the previous experiment. Applying the same concept that separation causes a loss in efficiency and power, our purpose becomes to reduce and delay its formation. This is accomplished by diverting the slow-moving fluid away so as to let its place be occupied by a faster stream of fluid which will reduce the boundary-layer buildup and thus decrease separation.

To control the boundary layer in the centrifugal impeller, slots in the impeller blading at the point of

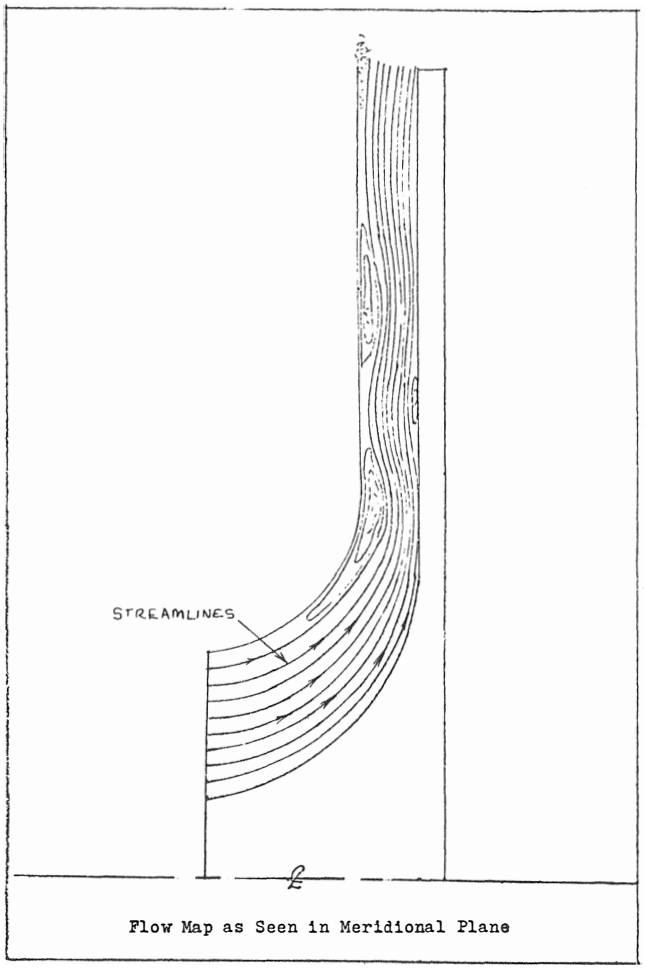

Figure 7. Flow Map as Seen in Meridional Plane.

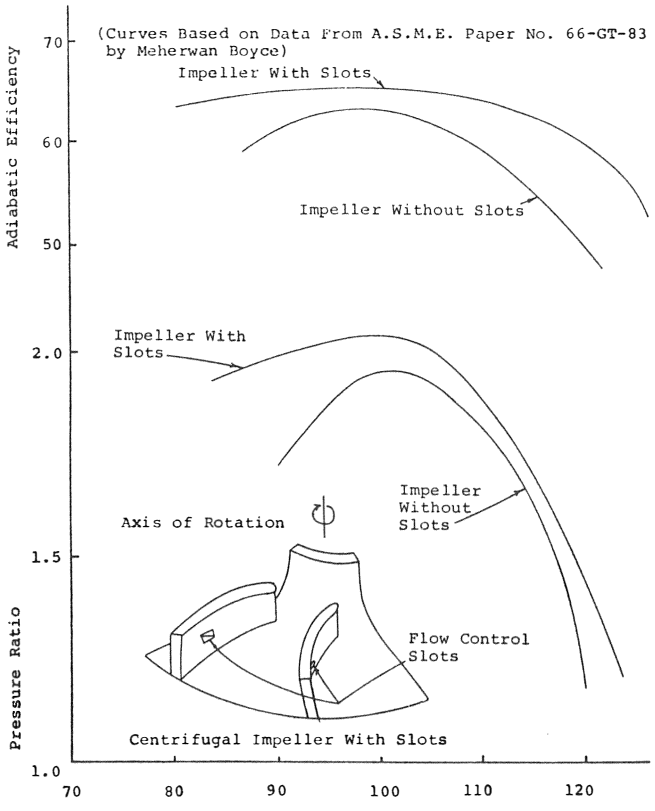

Figure 8. Percent Design Flow—Laminar Flow Control-Centrifugal Impeller.

separation were used. To realize the full capability of this system, these slots should be directional and converging in a cross-sectional area from the pressure to the suction sides (Figure 8). The fluid so diverted by these slots increases in velocity and attaches itself to the suction sides of the blades. This results in moving the separation region closer to the tip of the impeller, thus reducing slip and losses encountered by the formation of large boundary-layer regions.

To indicate the soundness of this theory, a simple experiment was conducted with a different impeller using air as the fluid medium. The slots were located at the point of separation of the flow from the blades. This point of separation was located using the flow visualization technique developed in this paper. The slots decreased in area from the pressure to the suction side. Experimental results indicated improvement in pressure ratio, efficiency, and surge characteristics of the impeller (Figure 8). The adiabatic efficiency herein referred to is calculated as follows:

$$\text{Adiabatic efficiency} = \frac{T_{in}\left[(PR)^{\frac{\gamma-1}{\gamma}}-1\right]}{\Delta T} \tag{26}$$

where T = temperature, PR = pressure ratio, γ = specific heat ratio, and ΔT = temperature rise.

Recent work done by Rodgers indicates that other methods to improve the critical surge-to-stall margin can be also achieved by increasing the impeller sweepback in the case of centrifugal compressors. Other attempts have been in the area of sucking the boundary layer in the vaneless diffuser, but this does lead to a slight decrease in efficiency due to loss of flow.

RADIAL INFLOW COMPRESSOR

New developments in compressor aerodynamics would not be complete without mention of the radial inflow compressor. The radial inflow compressor and its counterpart, the radial outflow turbine, have been to many fluid dynamists, a paradox of their logical form of thinking. However, the earliest turbine in recorded history is an outward flow turbine credited to Hero some 200 years ago. The earliest successful hydraulic turbines were outward flow, and the first turbines installed at Niagara Falls were also outward flow turbines. There is, however, no such history one may fall back on for the case of the radial inflow compressor.

In recent years, there has been some interest shown for this type of compressor. A compressor was built and tested by H. Petermann (27);[1] however, due to low efficiencies, the compressor did not gain much support. Recent patent disclosures by Gregory (28) have revived interest in this type of a compressor as a source of air for small auxiliary power units; however, this study does not analyze his patent disclosure but is general in scope. The advantages put forth for such a compressor are its multiple staging capability with a radial outflow compressor. This is demonstrated in Figures 9 and 10.

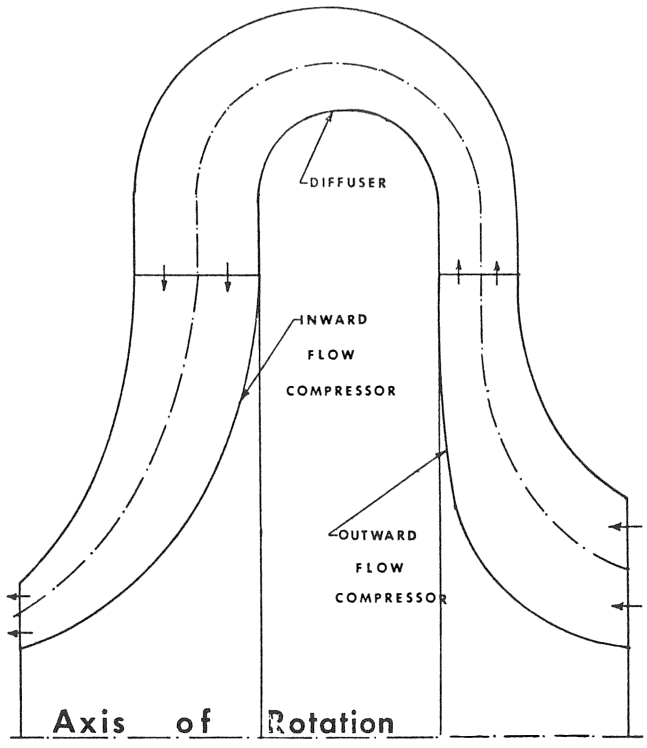

Figure 9. Stage Compressor Showing an Outward and Inward Flow Compressor.

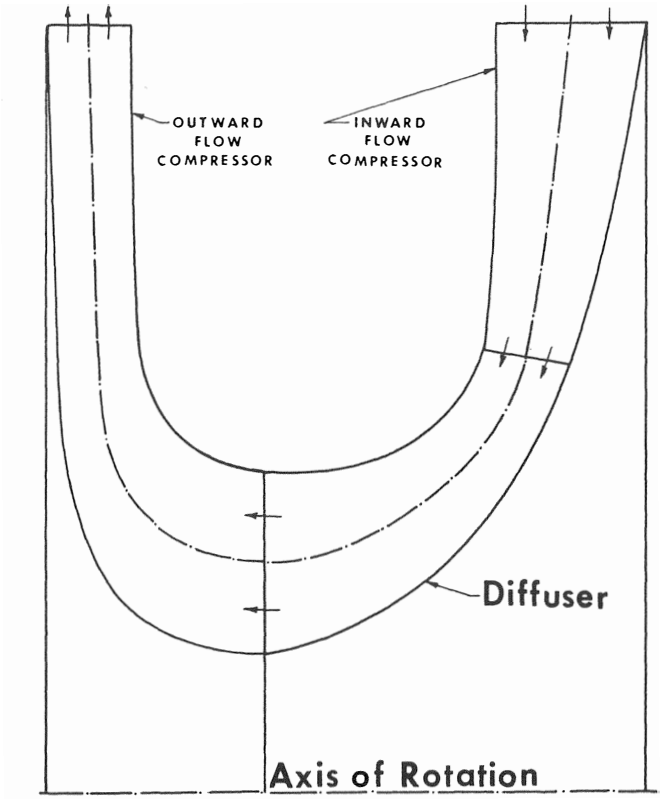

Figure 10. Stage Compressor Showing an Inward and an Outward Flow Compressor.

The advantages, obvious from the figures, are compactness and a smooth transition from one stage to the other. Losses are relatively high when two radial outflow stages are coupled. However, this does not necessarily mean that the combination of a radial outflow and radial inflow compressor is more efficient. The goal of a study conducted by Boyce and Bale (29) was to evaluate this combination and present the findings based completely on a theoretical investigation.

The first step in investigating the feasibility of the radial inflow compressor was to check it against the Euler turbine equation:

$$E = m\,(U_1V_{\theta 1} - U_2V_{\theta 2}) \qquad (27)$$

The only requirement here is that for a compressor, the product of $U_2V_{\theta 2}$ must be greater than $U_1V_{\theta 1}$, since in the case of the radial inflow compressor, $U_1 > U_2$, the centrifugal effect is opposing the flow. To overcome this, many varied approaches are possible. A radial fluid entry, no whirl, would give $V_{\theta 1} = 0$. The absolute exit velocity can be increased giving a large value of $V_{\theta 2}$; however, this has some undesirable effects due to the conversion of this large kinetic head to a pressure head. Regardless of the design, it is obvious that the radial inflow compressor is theoretically feasible. Its performance is another question.

The conclusion of the study was that for about a 3 : 1 pressure ratio. The estimated efficiency is about 70 percent. The blade loading seems to be good, and the problem of flow separation a minimum. The theory developed predicted Petermann's (27) compressor performance closely; thus, giving confidence in the approach developed. Presently, all test models have had the diffuser and the rotor in the radial direction. The studies here indicate that better efficiencies would be obtained if the rotor discharged in the axial direction. Thus, the conclusion drawn was that with more development it could provide an alternate compact high pressure gas source.

REFERENCES

1. Wu, Chang Hua, "A General Theory of Three Dimensional Flow in Subsonic and Supersonic Turbomachines of Axial, Radial, and Mixed-Flow Types," NACA TN 2604, 1952.
2. Stanitz, J. D., and Prian Vasily D., "A Rapid Approximate Method for Determining Velocity Distribution on Impeller Blades of Centrifugal Compressors," NACA TN 2421, 1951.
3. Hamrick, J. T., Kimsburg, Ambrose, and Osborne, Walter, "Method of Analysis for Compressible Flow Through Mixed Flow Centrifugal Impellers of Arbitrary Design," NACA Report 1082, 1952.
4. Dallenbach, F., "The Aerodynamic Design and Performance of Centrifugal and Mixed Flow Impellers."
5. Stockman, N. O., and Kramer, J. L., "Method for Design of Pump Impellers Using a High Speed Digital Computer," NASA TN D 1562, 1963.
6. Boyce, M. P., and Bale, Y. S., "A New Method for the Calculations of Blade Loadings in a Radial Flow Compressor," ASME Paper No. 71 - GT - 60.
7. Vavra, M. H., Aerothermodynamics and Flow in Turbomachines, Wiley, New York, 1960.
8. Watabe, K., "Experiments on Fluid Friction of Rotating Disc with Blades, "Japan Society of Mechanical Engineers, Bulletin, Vol. 5, No. 17.
9. Watabe, K., Japan Society of Mechanical Engineers, Bulletin, Vol. 7, Nov. 26, 1966.
10. Watabe, K., "Effects of Clearances and Grooves on Fluid Friction of Rotating Discs," Japan Society of Mechanical Engineers, Bulletin, Vol. 8, No. 29, Feb. 1965, pp. 55-63.
11. Schmieden, C., Uber den Widerstand einer in einer Flussigkeit rotierenden Scheibe, ZAMM 8, 1928, pp. 460-479.
12. Schulz-Grunow, F., Der Reibengswiderstand rotierender scheiben in gehausen, ZAMM 15, 1935, p. 191.
13. Balje, O. E., "Loss and Flow Path Studies on Centrifugal Compressors—Part I, "ASME Paper No. 70 - FT - 12a
14. Balje, O. E., "Loss and Flow Path Studies on Centrifugal Compressors—Part II," ASME Paper No. 70 - GT - 12b

15. Boyce, M. P., and Bale, Y. S., "Diffusion Loss in a Mixed Flow Compressor," Paper No. 729061, Intersociety Energy Conversion Engineering Conference, San Diego, September 1972.

16. Eckert, B., Axial and Radialkompressoren, Springer, 1953.

17. Sherstyuk, A. N., et al., "Influence of Clearances between the Impeller Blades and the Casing on the Characteristics of the Blower of a Motor Car Turbo Compressor," (Vliyanie zazora mezhdu lopatkami kolesa i korpusom na kharakteristiki nagnetatelya avtomobil' nogo turbokompressora).

18. Vasil'ev, V. P., et al., "Investigation of the Influence of the Axial Clearance on the Characteristics of a Centrifugal Compressor," Teploenergetika, Vol. 16, No. 3, 1969. pp. 69-72.

19. Boyce, M. P., "A Practical Three-Dimensional Flow Visualization Approach to the Complex Flow Characteristics in a Centrifugal Impeller," *Journal of Engineering for Power*, Trans. ASME, Paper No. 66-GT-83.

20. Fowler, H. S., "An Investigation of the Flow Processes in a Centrifugal Compressor Impeller," NRCC ME-220, Ottawa, July 1966.

21. Fowler, H. S., "Experiments on the Flow Processes in Simple Rotating Channels," NRCC ME-229, Ottawa, January 1969.

22. Senoo, Y. and Nakase, Y., "An Analysis of Flow Through a Mixed Flow Impeller," ASME Paper No. 71-GT-2, April 1971.

23. Senoo, Y. and Nakase, Y., "A Blade Theory of an Impeller with an Arbitrary Surface of Revolution," ASME Paper No. 71-GT-17, April, 1971.

24. Katsanis, T., "Use of Arbitrary Quasi-Orthogonals for Calculating Flow Distribution in the Meridional Plane of a Turbomachine," NASA TND-2546, December, 1964.

25. Schiller, L., "Uber den Stromungswiderstand von Rohren Verschiedenen Querschnitts und Rauhigkeitsgrades," ZAMM, Vol. 3, 1923, pp. 2-13.

26. Nikurdse, J., "Turbulente Stromung in Nicht Kreisformigen Rohren," Ing-Arch., Vol. 1, Germany, 1930.

27. Petermann, H., Untersuchungen am Zentsipetalrad fur Kreiselverdichter Forschung, Vol. 17, 1952.

28. Gregory, A. T., "Elastic Fluid Compressor," United States Patent Office, 3305165, February 21, 1967.

29. Boyce, M. P. and Bale, Y. S., "Feasibility Study of a Radial Inflow Compressor," ASME Paper No. 72-GT-52, April 1972.

30. Stahler, A. F., "The Slip Factor of a Radial Bladed Centrifugal Compressor," ASME Paper No. 64-GTP-1, March 1964.

31. Dallenbach, F., "The Aerodynamic Design and Performance of Centrifugal and Mixed-Flow Compressors," 1961 SAE International Congress, January 1961.

32. Wiesner, F. J., "A Review of Slip Factors for Centrifugal Impellers," Journal of Engineering for Power, Trans. ASME, P. 558-572, October 1967.

33. Wood, G. M., Welma, H., Lamers, R. P., "Tip-Clearance Effects in Centrifugal Pumps," *Journal of Basic Engineering*, Trans. ASME, P. 932-940, December 1965.

34. Sheperd, D. G., Principle of Turbomachinery, MacMillan, New York, 1957.

35. Vincent, E. T., The Theory and Design of Gas Turbines and Jet Engines, McGraw-Hill, New York, 1950.

36. Owezarek, J. A., Fundamentals of Gas Dynamics, International Textbook Co., Pennsylvania, 1968.

37. Balje, O. E., "A Contribution to the Problem of Designing Radial Turbomachines," Transactions of the ASME, 1952, p. 468.

38. Rodgers, C., "Influence of Impeller and Diffuser Characteristics and Matching on Radial Compressor Performance," Solar Aircraft Co., Paper No. 268B.

39. Honami, S., Tsukagoshi, K., Watanabe, I., "Investigation Concerning the Fluid Flow in the Mixed-Flow Diffuser," ASME Paper No. 71-GT-40, April, 1971.

NOMENCLATURE

$a_o = \sqrt{\gamma R T_o}$

$a, b, c,$ = constants (geometric parameter)

b_i = inlet width

B = blade shape parameter

C_f = coefficient of friction

d = diameter

d_H = hydraulic diameter

$\frac{D'}{Dt} = \frac{D}{Dt} - \vec{\omega x}$

E = theoretical available energy

F = constant of integration

h = enthalpy

H = form factor

J = constant in differential equation

K = polytropic constant $= (\eta\gamma)/[1-\gamma(1-\eta)]$

L = constant in differential equation

M_{rel} = relative Mach number

m = length along meridional line

m = mass flow rate

n = length along normal to meridional line

N = number of streamtubes

P = static pressure

Δq = loss in the flow passage

q = head

Re = Reynolds number (based on blade speed and diameter of impeller)

Re_a = Reynolds number (based on average velocity and hydraulic diameter)

r = radial distance from axis of rotation

r_c = radius of curvature of meridional streamline

t = time

t_θ = blade thickness in circumferential direction

T = static temperature

V = absolute fluid velocity

W = relative fluid velocity

U = blade speed

z = axial distance from impeller inlet

Z = number of blades

Greek Symbols

α = angle meridional streamline makes with impeller axis

β = blade angle

δ = momentum thickness

l = meridional path length

μ = deceleration ratio (W_2/W_1)

η = polytropic efficiency

η_{imp} = impeller efficiency

Θ = angular distance from radial line rotating with impeller

ρ = density

ϕ = function in differential equation

σ = solidity factor

ω = rotative speed of impeller

Subscripts

avg = average

BL = blade loading

c = clearance

D = driving surface to blade

DF = disk friction

e = rotor exit

ex = diffuser exit

h = hub

i = rotor inlet

ia = adiabatic

j = streamline being calculated

j−1 = known streamlines

o = stagnation conditions

oa = overall theoretical

OSF = vaned or vaneless diffuser

r = radial component

rc = recirculating

s = shroud

SF = skin friction

sh = shock

th = theoretical

tot = theoretical total

T = trailing surface to blade

vd = vaned diffusers

VLD = vaneless diffuser

w = wake mixing

z = axial component

θ = circumferential component

1 = inlet of rotor

2 = outlet of rotor

3 = exit of vaneless diffuser

4 = exit of vaned diffuser